Coupling a point-like mass to quantum gravity with causal dynamical triangulations

I Khavkine, R Loll, P Reska

ITP-UU-09/59
SPIN-09/49

Coupling a Point-Like Mass to Quantum Gravity with Causal Dynamical Triangulations

I. Khavkine, *R. Loll* and *P. Reska* [1]

Spinoza Institute and Institute for Theoretical Physics,
Utrecht University,
Leuvenlaan 4, NL-3584 CE Utrecht, The Netherlands.

Abstract

We present a possibility of coupling a point-like, non-singular, mass distribution to four-dimensional quantum gravity in the nonperturbative setting of Causal Dynamical Triangulations (CDT). In order to provide a point of comparison for the classical limit of the matter-coupled CDT model, we derive the spatial volume profile of the Euclidean Schwarzschild-de Sitter space glued to an interior matter solution. The volume profile is calculated with respect to a specific proper-time foliation matching the global time slicing present in CDT. It deviates in a characteristic manner from that of the pure-gravity model. The appearance of coordinate caustics and the compactness of the mass distribution in lattice units put an upper bound on the total mass for which these calculations are expected to be valid. We also discuss some of the implementation details for numerically measuring the expectation value of the volume profiles in the framework of CDT when coupled appropriately to the matter source.

[1] email: i.khavkine@uu.nl, r.loll@uu.nl, p.m.reska@uu.nl

1 Introduction

There has been growing interest in a nonperturbative formulation of quantum gravity in recent decades. Several candidate theories have emerged, among which is the Causal Dynamical Triangulations (CDT) programme. This approach implements a nonperturbative path-integral quantization of gravity, where each contributing spacetime history carries a well-defined causal structure. In one of the phases of the underlying statistical model of 'random geometry' one has observed the formation of an extended universe with good classical properties. More specifically, it has been shown that both its Hausdorff [1] and spectral dimension [2] are four on large scales. Furthermore, the large-scale shape of this dynamically generated background geometry matches to great accuracy that of a de Sitter universe [3], corresponding to a universe with a positive (renormalized) cosmological constant, and the quantum fluctuations around it agree with predictions from a mini-superspace model [4].

As a next step towards making the model more realistic, we want to study matter coupling using CDT. In the framework of dynamical triangulations, it is straightforward to set up dynamical, coupled gravity-matter systems by extending the sum over all geometries to a double-sum over all geometrical *and* matter field configurations (for a spin, scalar or gauge field, say). This has already been demonstrated in the corresponding *Euclidean* quantum gravity models in four dimensions [5, 6, 7, 8, 9]. The situation we will be studying presently is slightly different, and assumes that a particular matter configuration has already been arrived at, namely, one that can be approximated by a compact mass distribution that we shall refer to as a *point-like mass*. Compared with the matter-free case, this introduces an inhomogeneity in the geometry of the spatial slices, but preserves spherical symmetry. Such a situation is of great physical relevance because it corresponds to the gravitational field of any spherically symmetric mass distribution in a universe with a positive cosmological constant.

The relevant classical solution to the Einstein equations outside the source is given by the Schwarzschild-de Sitter (SdS) metric. In this paper, we address the question of how to detect the presence—on sufficiently large scales—of this particular background geometry in CDT quantum gravity coupled to a point-like mass. This implies finding a quantum observable that is well defined in the nonperturbative, background-independent setting of the full path integral, is sensitive to the presence of the mass, and is potentially measurable in the computer simulations. The dynamics of CDT quantum gravity is defined directly on the space of geometries (in a continuum language: the space of metrics modulo diffeomorphisms) and forces one to tackle the issue of observables head-on, by giving measuring prescriptions for geometric observables whose expectation values with respect to the ensemble average over all spacetime geometries give nontrivial results. Examples of this are the dynamical dimensions mentioned above.

In the CDT setting, another class of geometric quantities is accessible relatively easily, namely, those referring to the proper-time slicing that comes with the formulation.[2] This has been used previously in the pure-gravity theory to study both

[2]One should keep in mind that geometric quantities associated with a spatial slice in the simulations will in general not correspond directly to properties of classical three-geometry; for this, they will usually need to be smeared out (coarse-grained) over some finite time-extension, cf. [10]. However, the spatial three-volume considered below is a sufficiently robust quantity, for which this turns out not to be necessary.

the *volume profile* (the development $V_3(\tau)$ of the spatial three-volume as function of proper time τ) and the correlator of quantum fluctuations in the three-volume around the dynamically generated de Sitter background spacetime [3, 4]. As we shall see, the volume profile is a geometric quantity that is modified by the presence of the mass. We shall focus in this work on the derivation in the continuum of the volume profile of the Euclidean Schwarzschild-de Sitter (ESdS) solution in a proper-time slicing, which may be compared to the values obtained from CDT simulation. To our knowledge, no background-independent approach to quantum gravity has so far succeeded in generating a Schwarzschild-de Sitter geometry in the classical limit. The volume profiles we derive can be used as a criterion to identify this spacetime in any background-independent approach to quantum gravity in four spacetime dimensions, when using a suitable proper-time slicing.

Unlike the previously mentioned work on dynamical matter fields, very little has been done on coupling point or point-like masses to quantum gravity in four dimensions. We are not aware of any nonperturbative, background-independent approach to quantum gravity that has been *ab initio* coupled to point masses in four dimensions. Inclusion of point particles is common in discussions of both classical and quantum three-dimensional gravity [11]. The three-dimensional theory has no local degrees of freedom and therefore is significantly different from the four-dimensional one, already at the classical level. The inclusion of point particles is simplified by the fact that their presence only creates conical defects [12, 13], and not stronger curvature singularities like in higher dimensions. Quantization of three-dimensional gravity with point particles has been discussed early on in [14, 15] and more recently in the contexts of Loop Quantum Gravity [16] and the Ponzano-Regge Spin Foam model [17]. In four dimensions, a spherically symmetric quantum spacetime has been studied in a series of papers by Husain and Winkler [18, 19, 20], where they applied canonical quantization to a symmetry-reduced midi-superspace model of black hole collapse from a scalar field coupled to gravity. The Euclidean Schwarzschild-de Sitter space, which we discuss extensively below, has been studied in the context of black hole thermodynamics [21] and the stability of de Sitter space [22, 23]. Schwarzschild-de Sitter space shares many of its global properties with de Sitter space. An overview of the latter can be found in [24].

In this work, we propose to perform CDT simulations with a mass line representing the point-like source and measure the average volume profile to test whether the classical limit of CDT coincides with the Euclidean Schwarzschild-de Sitter geometry. We derive the expected deviation from the Euclidean de Sitter profile for pure gravity by performing a proper-time slicing of the continuum ESdS geometry glued to an interior matter region. The particular Gaussian normal coordinate system we work with in the continuum, in order to mimic the CDT set-up, exhibits caustics in the vicinity of the mass, which cannot be eliminated by extending the coordinates to the matter region. For the numerical derivation of the volume profiles, we neglect this problematic region by cutting out a tube from the Euclidean Schwarzschild-de Sitter space whose spatial slices are balls of constant Schwarzschild radius. This procedure gives rise to an upper bound for the mass under consideration. The profiles for masses below this bound are the ones that should be compared with those coming from CDT simulations to test for the possible presence of an ESdS ground state. A mass propagating in triangulated spacetime can be represented by a timelike mass line on the lattice dual to the triangulation. Our analysis reveals that in order to compare the results derived here with those coming from simulations, the mass line should be

implemented so as to form a contractible loop on S^4 (or a suitable analogue on the $S^3 \times S^1$-topology used in simulations).

The paper is organized as follows. In section 2 we review CDT, emphasizing its hypersurface structure and its classical limit and describe the possibility to couple a point-like mass. Section 3 deals with the properties of ESdS space. Starting from the metric in static form we construct Gaussian normal coordinates to obtain a particularly simple proper-time form of the metric. In section 4 we derive the bound on masses accessible in simulations and derive the volume profiles of the ESdS geometry in the proper-time slicing for masses below this bound. Section 5 contains the conclusion and the outlook. Appendix A contains the technical details of the derivation of the metric in proper-time form. In Appendix B we discuss the matching of an interior matter solution to the exterior vacuum solution.

2 Causal Dynamical Triangulations

2.1 Regularization of the gravitational path integral

For readers unfamiliar with the quantization programme of Causal Dynamical Triangulations, let us briefly review its motivation, implementation and the main results it has produced to date (for more in-depth reviews, see [25, 26, 27, 28, 29]).

Building on insights from general relativity and (canonical) quantum gravity, this approach uses nothing but standard quantum-field theoretic principles and methods, adapted to the situation where geometry is no longer part of a fixed background structure, but is itself dynamical. The basic quantum-dynamical principle it implements is the Feynman path integral, the "superposition of gravitational amplitudes" or "sum over histories"

$$Z = \int\limits_{[g]\in\mathcal{G}} \mathcal{D}g \; \mathrm{e}^{iS^{\mathrm{EH}}[g]}, \quad \text{with} \quad S^{\mathrm{EH}} = \frac{1}{G_N}\int d^4x\sqrt{\det g}(R-2\Lambda), \tag{1}$$

where each history is a spacetime geometry (a diffeomorphism equivalence class $[g]$ of metrics on a fixed manifold M, with $\mathcal{G}$ the space of all such equivalence classes), weighted with the exponential of i times its Einstein-Hilbert action. Because of the nonrenormalizability of gravity as a perturbative quantum field theory on a Minkowskian background, such a path integral necessarily has to be nonperturbative, which means that it must include spacetime configurations "far" from any classical solution. The evaluation of the ensuing, highly non-Gaussian path integral is technically challenging, and in the CDT approach is addressed by using powerful lattice methods, borrowed from the nonperturbative treatment of QCD. Adapting them to gravity implies that the rigid lattices of gauge theory become themselves dynamical, and actually take the form of *dynamical triangulations*, because of the way the infinitely many geometric/curvature degrees of freedom of the theory are regularized.

Namely, the gravitational path integral is regularized by summing over a class of piecewise flat four-manifolds, which can be thought of as being assembled from (two types of) four-dimensional simplices, which are simply triangular building blocks cut out of Minkowski space. They are individually flat, but can pick up nontrivial deficit angles after being glued together pairwise along three-dimensional subsimplices (tetrahedra), with curvature concentrated at two-dimensional subsimplices (triangles) where tetrahedra meet. This does not imply that spacetime is conjectured to consist

of (Planck-sized) triangular building blocks. On the contrary, the edge length of the simplices serves as a short-distance cut-off and we are only interested in the *universal* properties of the model as this cut-off is sent to zero.

When evaluating the path integral, these simplicial geometries are taken to be Euclidean, like those that are summed over in the Euclidean gravitational path integral in its standard definition [30]. In contrast to previous Euclidean quantum gravity work, the triangulations used in CDT have a preferred, discrete notion of time $\tau = 1, 2, 3, \ldots$ inherited from a class of triangulated Lorentzian piecewise flat spacetimes by explicit Wick rotation [31, 32]. In the Lorentzian regime, the triangulations are restricted to those consisting of a sequence of slices with (discrete) proper-time thickness $\Delta\tau = 1$ and fixed topology. Links that lie in a spatial hypersurface of constant integer τ are spacelike and links connecting two adjacent spatial slices of this kind are timelike. The restriction on the path integral histories is motivated by the desire to eliminate the causality-violating 'baby universes' in the time direction produced in *Euclidean* dynamical triangulations [33], which lead to an incorrect classical limit because of the absence of an extended four-dimensional geometry on large scales. After discretization and Wick rotation, the path integral becomes a statistical sum with Boltzmann weights using the Regge action [34], which is the discretized version of the Einstein-Hilbert action. The first major result of the CDT formulation was to show in exactly solvable two-dimensional quantum gravity that the signature, i.e., sum over Lorentzian as opposed to Euclidean geometries in the path integral, leads to genuinely different properties of the model (different intrinsic Hausdorff dimension, for instance) [35].

In dimension four, the regularized path integral can no longer be evaluated by exact methods, but Monte Carlo methods must be used to explore its continuum limit. This has led to a number of unexpected and new results. Since the curvature is allowed to fluctuate strongly on short scales, and since a nontrivial limiting process is involved, it turns out that the dimensionality of the "quantum geometry" generated by the path integral is not necessarily four. Only when the summed triangulations have the causal structure described above, and the (bare) coupling constants are chosen appropriately, does a four-dimensional universe emerge from the quantum theory [1, 10]. This is the first instance in which a classical-looking universe has been obtained from first principles within a nonperturbative formulation of quantum gravity. Moreover, as already mentioned in the introduction, this dynamically generated universe macroscopically resembles a de Sitter universe, with matching quantum fluctuations [3, 4].

2.2 Time slicing and classical limit of CDT

The classical limit of the CDT model is considered good if, when the length scale is large and quantum fluctuations are small, the continuum limit of the regularized path integral reproduces the observable predictions of classical general relativity. In order to compare the two, one needs to phrase their respective results in a common language, that of geometric *observables*. These are generally hard to come by, but in the case of CDT quantum gravity there is an extra structure that comes to our help. Each sample CDT geometry in the regularized path integral carries a discrete time label. Since this labelling is respected by the quantum superposition, a (possibly rescaled) version of the discrete time parameter labelling the slices is still available in the continuum. The reason for calling this a *proper* time comes from the fact that (i) at the discretized level, inside each flat four-simplex one can introduce a proper-time slicing (with respect to the Minkowskian metric of the simplex) in a way that after

gluing all of them together, the triangulated "sandwich geometry" between integer times τ_0 and $\tau_0 + 1$ can be foliated into hypersurfaces $\tau = const$, $\tau_0 \leq \tau \leq \tau_0 + 1$ [36], (ii) in the continuum limit, the volume profile of the extended universe emerging in the 'well-behaved' phase of CDT quantum gravity matches that of a continuum Euclidean de Sitter space as a function of cosmological proper time, if the bare τ of the regularized geometries is rescaled by a finite constant. More precisely, the expectation value of the volume profile behaves to a very good approximation as

$$\langle V_3(\tau) \rangle = A \cos^3 (\tau/B) \,, \tag{2}$$

for some constants A and B depending on the bare coupling constants and geometric parameters of the triangulation (see [4] for further details). The volume profile of Euclidean de Sitter space has exactly the same shape [cf. equation (12) below].

The latter is of course a highly nontrivial result, however, one needs to keep in mind that the role of τ as (constant multiple of) proper time—in the way this notion is used in the classical continuum theory—emerges unambiguously from CDT only on sufficiently large scales and in the sense of a quantum average (of a particular quantum observable). In order to understand better the relation with the continuum situation, recall that in the classical theory geometries with a time foliation are naturally described in the ADM formalism [37]. Labelling the spatial slices of the foliation as hypersurfaces of constant time t, and choosing coordinates x^i on each of them, the geometry is specified by writing the metric in the ADM form,

$$ds^2 = -N(t,x)^2 dt^2 + h_{ij}(t,x)(dx^i + N^i(t,x)dt)(dx^j + N^j(t,x)dt), \tag{3}$$

with lapse function $N(t,x)$, shift vector $N^i(t,x)$ and spatial metric $h_{ij}(t,x)$. The volume profile of the spacetime with respect to this foliation is then given by

$$V_3(t) = \int d^3x \, \sqrt{\det h}. \tag{4}$$

A metric in proper-time form is one where $N = const$. Requiring in addition the shift vector N^i to vanish, so that there are no cross terms $dx^i dt$ and the gauge is essentially fixed, one obtains a metric in *proper-time gauge* [38, 39]. The associated coordinates are the same as Gaussian normal coordinates [40, 37] with respect to any of the spatial hypersurfaces. Although such coordinate systems can always be set up in the neighbourhood of a hypersurface, they rarely exist globally because of the formation of caustics.[3] Therefore, taking a path integral only over those smooth metrics which globally can be put into proper-time gauge would appear far too restrictive.

However, this is not what is done in CDT quantum gravity, assuming we identify the time t in (3) with CDT's τ-parameter. Firstly, the ADM-decomposition (3) for differentiable, metric manifolds cannot in general be extended beyond a single four-simplex in piecewise flat simplicial geometries; they are neither smooth nor differentiable. (The same holds for individual CDT three-slices.) Secondly, when one follows the geodesics of freely falling, initially hypersurface-orthogonal observers in CDT (which are still well defined in open neighbourhoods not containing curvature singularities), one finds that they generically form caustics within a single time step

[3]Even in flat Minkowski space, by choosing an initial hypersurface $\tau = 0$ with typical extrinsic curvature K, caustics will form after a typical evolution time $\tau \sim K^{-1/2}$. For instance, a sphere of radius R has $K \sim 1/R^2$, while Gaussian normal coordinates, extended to the interior, become singular at its centre.

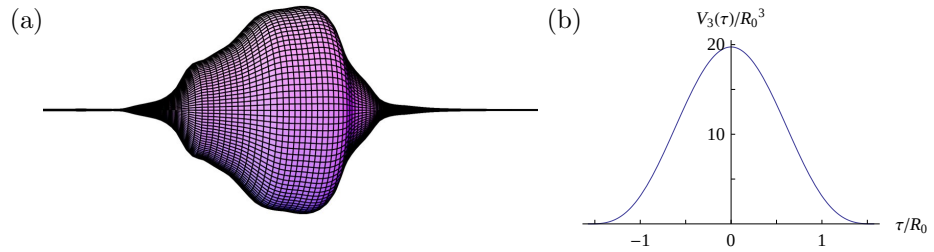

Figure 1: (a) Volume profile of a typical CDT universe that contributes to the sum over triangulations, made into a solid of revolution by rotation about the proper-time axis. It consists of an extended region, the 'blob', and a degenerate tube. (b) Normalized volume profile $V_3(\tau)/R_0^3$ for EdS space, cf. equations (2) and (12), which after a constant rescaling of τ matches that of the expectation value $\langle V_3(\tau)\rangle$ determined in CDT simulations [3, 4].

$\Delta\tau = 1$. From this point of view, CDT histories are indeed full of caustics (and curvature singularities), whose density only increases as the lattice cut-off is taken to zero. Since individual path integral histories are *not* physical, this in no way contradicts the possibility that their *nonperturbative superposition* can be a quantum geometry which on large scales behaves classically. As we have seen for the case of Euclidean de Sitter space (EdS), the ground state of the empty universe emerging from CDT, it is also no obstacle to the existence of a well-defined global description in proper-time gauge. The fact that Euclidean de Sitter space possesses a global proper-time form which moreover has a direct Lorentzian interpretation under the straightforward substitution $\tau \to -i\tau$ is in a way a fortunate circumstance. If we want to use CDT quantum gravity to describe different physical situations, associated with a specific matter content and/or boundary conditions, we would in general expect that making a link to Lorentzian continuum physics will be (much) more difficult.

As we will see in subsequent sections, the inclusion of a mass distribution already presents challenges of this kind. Nevertheless, by requiring the mass distribution to be sufficiently compact (point-like), the total mass M to be small and treating the situation as a one-parameter family deviating from the known, pure-gravity case $M = 0$, we are able to quantify the consequences of $M \neq 0$ for the physical volume profile.

Before describing the inclusion of such a point-like mass, let us comment on space-time topology. Computer simulations of CDT in four dimensions are performed with compact manifolds of product topology $I \times \Sigma^{(3)}$ or, if for simplicity the time direction is compactified, $S^1 \times \Sigma^{(3)}$. In simulations considered so far, the spatial slices were chosen to be topological three-spheres, $\Sigma^{(3)} = S^3$. Interestingly, in the pure-gravity case, despite fixing the topology to $S^1 \times S^3$ at the outset, the system is driven dynamically to a state which is as close to a four-sphere as allowed by the kinematical constraints (minimal, nonvanishing spatial diameter at each time step). This is illustrated in Fig. 1a, which shows the volume profile $V_3(\tau)$ of a typical sample geometry from the regularized path integral. It consists of an extended universe which forms a 'blob' and a thin degenerate tube or 'stalk' of minimal extension. After subtracting the minimal stalk-volume from the data, the average volume profile can be matched to that of EdS space (the "round four-sphere"), shown in Fig. 1b, with great accuracy. In simulations, the period of the time identification is much larger than the time extension of the universe, such that this result is unaffected by the periodic boundary

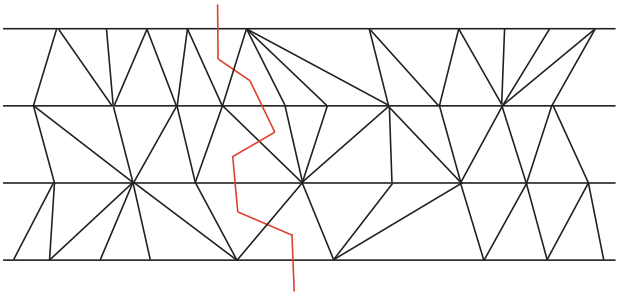

Figure 2: Mass line on the dual lattice of a triangulation in CDT, for simplicity demonstrated in two dimensions, representing the worldline of a point-like mass.

conditions.

2.3 CDT with a localized mass

We want to generalize the above discussion by including matter. More specifically, we are interested in the effect of a localized mass on the ground state geometry found in Causal Dynamical Triangulation simulations. The concept of a point mass is already problematic in classical general relativity, in the sense of including it consistently as a distributional source in the Einstein equations (for a recent overview, see [41] and references therein). We will refrain from making this idealization and assume an extended, but localized, spherically symmetric mass source, mostly without discussing its internal structure. An exception is Appendix B, where we consider the extension of the proper-time coordinates in the exterior to a simple interior matter distribution. In any case, from the point of view of the regularized geometries used in the simulations, one cannot really distinguish between a point mass and a compact, massive object that fits inside a single spatial simplex. In this context, we call a compact mass distribution *point-like* if its spatial extent does not exceed that of a single triangulation simplex.

In CDT simulations, the worldline of such a mass is naturally represented by a time-like path, transverse to the foliation, on the dual lattice of the triangulation, as illustrated in Fig. 2. The (Euclidean) action associated with this mass line is $S_p = ML$, where M is the bare mass, and L is the (positive) total length of the line in units of the lattice spacing a. This is the regularized version of the continuum action associated to a localized mass M, $S_p = M \int d\tau$, integrated with respect to the proper time along its world-volume, which in turn depends on the spacetime geometry containing the mass line. The action S_p gives an extra contribution to the Boltzmann weight of each path-integral configuration and therefore changes the expectation value of geometric quantities under consideration. In particular, the volume profiles are expected to be modified.—The remainder of this paper is devoted to the derivation in the continuum of the classical form of the modified volume profiles, which could be compared to the expectation values of corresponding quantities numerically obtained from CDT simulations.

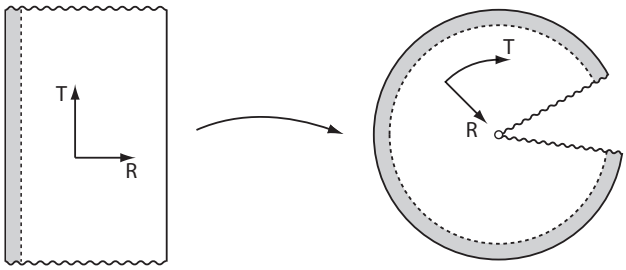

Figure 3: Euclidean Schwarzschild-de Sitter space can be compactified by taking the Schwarzschild time coordinate T to be periodic. The geometry can be smoothed out in the central point $R = R_{++}$ (the location of the cosmological horizon in Lorentzian signature) by adjusting the periodicity of T. The shaded region represents the matter region and contains no conical singularities. It is glued to the exterior vacuum solution at a constant Schwarzschild radius $R = R_S > R_+$, outside the horizon. The compactified, closed geometry has topology S^4.

3 Euclidean Schwarzschild-de Sitter space

3.1 Metric in static form

Written in the static form of the metric, the line element of Euclidean Schwarzschild-de Sitter (ESdS) space is

$$ds^2 = f(R)dT^2 + f(R)^{-1}dR^2 + R^2 d\Omega^2(\theta, \phi), \tag{5}$$

where $f(R) = 1 - 2M/R - R^2/R_0^2$, and the coordinates T and R are referred to as static or Schwarzschild coordinates. The mass of the source is M and $R_0 = \sqrt{3/\Lambda}$ with $\Lambda > 0$ being the cosmological constant. For a given cosmological constant, there is an upper limit for the mass of the Schwarzschild black hole, given by $M_N = 3^{-3/2}R_0$, the Nariai mass [42], because the static region disappears in this limit. We recover Euclidean de Sitter space for $M = 0$, and the Euclidean Schwarzschild metric for $\Lambda = 0$. The metric has Euclidean signature in the static region $R_+ < R < R_{++}$, where

$$R_+ = 6M_N \cos\left(\frac{\alpha + 4\pi}{3}\right), \quad R_{++} = 6M_N \cos\left(\frac{\alpha}{3}\right), \tag{6}$$

are the locations of the black hole horizon and the cosmological horizon, respectively, and $\alpha = \arccos(-M/M_N)$. Also, $R_+ \to 0$ and $R_{++} \to R_0$ as $M \to 0$.

For the Lorentzian version of the solution (5), the event horizon only forms if the object that generates the gravitational field is sufficiently dense. We shall consider a mass distribution that is glued to the exterior vacuum region such that no event horizon is present. For now we will focus solely on the properties of the vacuum region.

The topology of Euclidean de Sitter space is S^4. Suppressing the two angular variables θ and ϕ in (5) with $M = 0$, we see that the two-dimensional sheet spanned by T and $0 < R < R_0$ can be wrapped by taking T to be periodic, as displayed in Fig. 3 (depicting the general Euclidean Schwarzschild-de Sitter case). The resulting punctured disc has a potential conical singularity at its centre, $R = R_0$, which is smoothed out by a specific choice of the T-period, namely $4\pi/|f'(R_0)| = 2\pi R_0$. One obtains the complete Euclidean manifold (for $M = 0$ this is S^4, as we will make explicit below) by gluing a two-sphere of radius R_0 to the puncture boundary.

In the case of Euclidean Schwarzschild-de Sitter space with $M \neq 0$, the maximal Euclidean vacuum region is spanned by $R_+ < R < R_{++}$. Periodic compactification along the T-direction introduces a different global topology and two potential conical singularities at R_+ and R_{++}, which cannot be smoothed out simultaneously [43]. Fortunately, the new topology and the ambiguity in periodicity need not be dealt with if the manifold consists of an ESdS exterior and an interior matter region (shaded in Fig. 3), without an inner horizon. In this case, the periodicity is again uniquely fixed to $T_P = 4\pi/|f'(R_{++})|$, which smoothes out the geometry around $R = R_{++}$, and the topology remains S^4.

As a consequence of the compactification, the mass line closes to a contractible loop on the S^4. If one wants to compare with the calculations done in this paper, this should be taken into account when implementing the mass line in CDT simulations, rather than using a noncontractible loop which winds around the compactified time direction, say.

3.2 Metric in proper-time form

As has been pointed out already, the explicit derivation of the volume profile of the Euclidean Schwarzschild-de Sitter geometry has to be done by adopting a proper-time gauge. In order to achieve this form, we construct comoving or Gaussian normal coordinates (cf. [40, 37]) from the $T = 0$ surface, which for the matter-free case coincides with half of the 'equator' of S^4 and will in general form a time-symmetric hypersurface. This procedure has been previously carried out, in Lorentzian signature, for the de Sitter case in [44] and for the Schwarzschild case in [45].

We briefly describe the necessary calculations here, while referring the reader to Appendix A for the details. First, one has to integrate the radial geodesic equations, taking initial conditions that guarantee that the geodesics are perpendicular to and their proper time parameter vanishes on the $T = 0$ hypersurface. Then one chooses the proper time of these radial geodesics as a new time coordinate τ. The comoving radial coordinate, R_i (the subscript i stands for *initial*), can be introduced as the position $R(T = 0)$, i.e. labelling each geodesic with the value of R at which it intersects the $T = 0$ hypersurface. The resulting metric has proper-time form and is diagonal,

$$ds^2 = d\tau^2 + \frac{(\partial R/\partial R_i)^2}{f(R_i)} dR_i^2 + R(\tau, R_i)^2 d\Omega^2, \tag{7}$$

where the expression for the Schwarzschild coordinate $R(\tau, R_i)$ as a function of the new proper-time coordinates is known from equation (30). For the Euclidean de Sitter case we find the explicit expression

$$R(\tau, R_i) = R_i \cos(\tau/R_0) \tag{8}$$

and the metric line element becomes

$$ds^2 = d\tau^2 + R_0^2 \cos^2(\tau/R_0) \left[\frac{dR_i^2}{R_0^2 - R_i^2} + (R_i/R_0)^2 d\Omega^2 \right]. \tag{9}$$

3.3 Domain of comoving coordinates and caustics

It is well known that Gaussian normal coordinates in general fail to cover the entire underlying manifold. Below, we determine how much of the EdS and ESdS spaces can be covered by the coordinates constructed in the previous section.

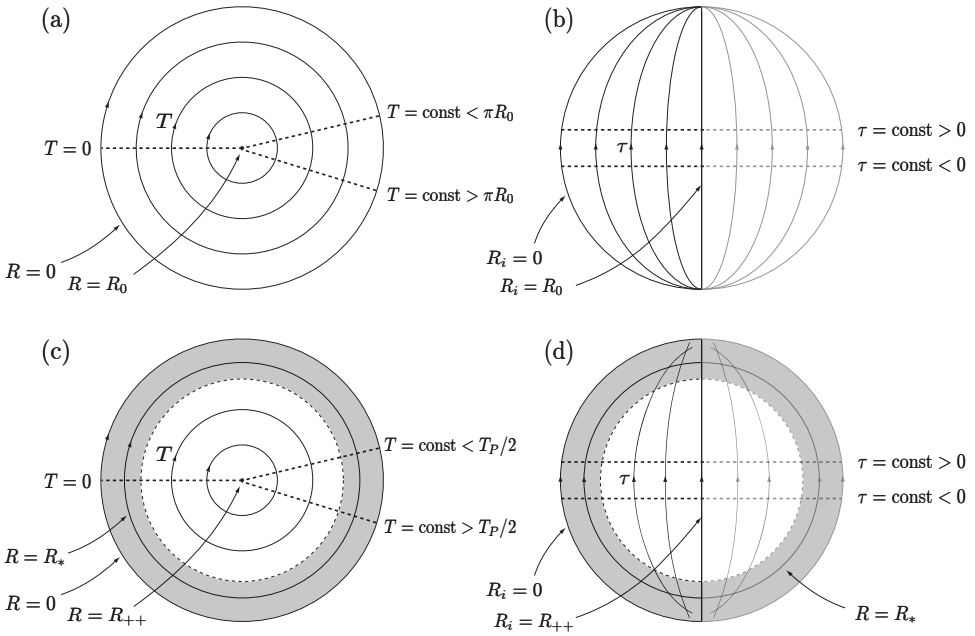

Figure 4: Euclidean de Sitter space (a, b) and Euclidean Schwarzschild-de Sitter space (c, d) (after periodically identifying the static time T, with angular variables θ, ϕ suppressed), described in terms of (a, c) static and (b, d) proper-time coordinates. The shaded region $R < R_S$ in (c, d) is occupied by matter. In static coordinates, lines $R = const$ are concentric circles, with mid point $R = R_{++}$ and outermost circle $R = 0$. In the proper-time coordinates, the lines $R_i = const$ converge at $\tau = \pm\pi R_0/2$ for (b), they start forming caustics in the region $R < R_*$ for (d). The middle line is $R_i = R_{++}$. Every $R_i = const$ appears once on the left half of the disc (dark curves, perpendicular to the $T = 0$ surface), and is mirrored on the right half of the disc (light curves, perpendicular to $T = T_P/2$).

First, we consider the simpler case of EdS space. The relationship between static (T, R) and comoving (τ, R_i) coordinates is illustrated in Fig. 4. The disc depicted in Fig. 4a is formed from R-T-space by periodically identifying the static time T such that $0 \leq T \leq 2\pi R_0$. The static coordinates (T, R) cover the entire disc. Lines of constant Schwarzschild radius R are concentric circles around the point $R = R_0$ (rather a two-sphere, with angular coordinates taken into account), which is added to the Euclidean manifold to make it complete. Fig. 4b depicts the same disc, but now with dark vertical lines representing constant R_i (radial geodesics) and dashed horizontal lines representing constant τ. Note that only half the disc is covered by Gaussian normal coordinates emanating from the $T = 0$ surface. The other half (which is of a lighter shade in the figure) can be covered by reflecting the (τ, R_i) coordinates about $R_i = R_0$ or, equivalently, by constructing Gaussian normal coordinates from the $T = \pi R_0$ surface, which smoothly joins the $T = 0$ one.

Figs. 4c and 4d parallel the above discussion for ESdS space, though the ranges of the static coordinates change to $0 \leq T \leq T_P$ and $0 < R < R_{++}$. Again, the right half of the disc in Fig. 4d can be covered by reflection of the (τ, R_i) coordinates or by constructing Gaussian normal coordinates from the $T = T_P/2$ surface. As explained in section 3.1 the geometry we are considering has no inner horizon since the exterior vacuum is matched to a static interior matter solution (shaded region) at $R_S > R_+$.

The comoving coordinate system breaks down at an intersection point of two radial geodesics, because it would associate two distinct labels (τ, R_i), (τ, R_i') with the same physical point. In Fig. 4b we see that the geodesics intersect only at the poles, $R = 0$ and $\tau = \pm\pi R_0$. In contrast, Fig. 4d shows that the geodesics intersect (form caustics) already for $R < R_*$. Fig. 4 is schematic, the corresponding calculations are presented in Appendices A and B. Therefore, we can conclude that comoving coordinates (τ, R_i) cover EdS space in its entirety[4], while only a portion of ESdS space is covered, namely for $R > R_*$, with R_* the boundary of the caustic region.

Caustics appear already in the ESdS exterior vacuum, in which case $R_* = (MR_0^2)^{\frac{1}{3}}$. Generically, caustics persist even if the vacuum exterior is glued to an interior matter solution of arbitrarily low density, as explicitly shown for a specific matter model in Appendix B. Thus, for convenience, from now on R_* will only refer to this *vacuum caustic boundary*. To ensure that the entire vacuum region is covered by comoving coordinates, we require that the matter-vacuum boundary satisfies the condition $R_S > R_*$, which puts an upper bound on the density of the mass distribution. We only consider densities below this critical value. This bound and the associated bound on the total mass are discussed in detail in sections 4.1 and 4.2.

We should emphasize that the occurrence of caustics does not imply any pathologies of the underlying spacetime, but is a consequence of the choice of a particular coordinate system. In order to calculate the volume profile, all we need is a proper-time slicing. Neither the vanishing of the shift vector nor the existence of a single, global coordinate system are in principle necessary. However, our (time-symmetric) choice of the Gaussian normal coordinates starting at $T = 0$ and $T = T_P/2$ has the advantage of being continuously connected to a globally well-defined coordinate system in the limiting case $M = 0$. That coordinate system was used to successfully compare classical, continuum volume profiles to those produced by CDT simulations. It is this successful case that we are 'perturbing' about.[5]

The global, proper-time coordinate system on de Sitter space is introduced by extending the range of the radial coordinate by introducing an angle ψ, $0 \leq \psi < \pi$, where

$$R_i = R_0 \sin\psi. \tag{10}$$

Every $R_i = const$ line appears twice on the disc in Fig. 4b. On the left half of the disc it is represented by an angle $\psi < \pi/2$ and on the right half by $\psi > \pi/2$, with the middle line given by $R_i = R_0$. The line element written in terms of τ and ψ becomes

$$ds^2 = d\tau^2 + R_0^2 \cos^2(\tau/R_0)\left(d\psi^2 + \sin^2\psi\, d\Omega^2\right). \tag{11}$$

Note that this is the line element of the round four-sphere, where the geodesic $R_i = 0$ has become the location of the coordinate singularity $\psi = 0$. Spatial sections of this four-dimensional Euclidean geometry are three-spheres, which is consistent with CDT simulations. From this metric, or already from the line element (9), we can immediately derive the volume profile

$$V_3(\tau) = 2\pi^2 R_0^3 \cos^3(\tau/R_0) \tag{12}$$

for EdS space, which we have referred to earlier in equation (2). We now turn to the calculation of the volume profile of ESdS space.

[4]Strictly speaking, these coordinates fail to cover some lower-dimensional submanifolds. But, since we are only interested in computing three- and four-volumes, they can be safely ignored.

[5]It is possible that there exist even more convenient coordinate choices for $M \neq 0$, which would avoid caustics altogether, but we have not found them.

4 Volume profiles

4.1 Cutting out the vicinity of the mass-line

In computer simulations, the volume profile is determined by counting spatial simplices per slice of constant proper time for the individual sample geometries and taking the average value over the ensemble. For simulations with a mass line, the average of the discrete geometries should approximate the Euclidean Schwarzschild-de Sitter space well away from the mass, but poorly close to it. Thus it makes sense to discard the simplices pierced by the mass line and to excise a corresponding thin 'tube' surrounding the mass from the four-dimensional continuum geometry. Only the volume profiles of the remaining regions will be compared. On every spatial slice $\tau = const$ we choose to cut out the region inside of a ball of a certain Schwarzschild radius R, whose area is $4\pi R^2$. Of course, this choice of the radius depends on the mass and only for small masses can we expect a good match between the continuum and discrete picture. A more detailed analysis on the mass bound will be presented in the following section.

An important property of this prescription is that the surface of this region (which has topology $S^2 \times S^1$ for compactified Schwarzschild time) is invariantly defined, and mapped into itself under the flow of the time-like Killing vector. This agrees with the discrete picture, where the sequence of four-simplices cut out of the four-geometry representing the mass line has the topology of a tube. A strict implementation of the classical continuum set-up on the simplicial lattice would allow only for mass lines whose boundary is everywhere time-like, which would limit the types of tube geometry that can occur in a single time step. This would be associated with an excised region per time step of some typical, average surface area $O(1)$ in discrete units, even though the internal geometry of the excised region is considered unspecified. Other prescriptions for cutting out the matter region in the classical continuum geometry are in principle possible. However, they must not deviate from the Schwarzschild prescription more than the scale set by the discretization (the lattice spacing) which is the size of the error already inherent in the triangulation procedure.

In view of the quantum nature of the CDT path integral, simulations may have to include more general mass lines, which can wind around longer in a given time step or are even allowed to run backwards in time.

4.2 Derivation of a mass bound

We emphasized that due to caustic formation in the continuum picture it is necessary to cut out a certain region of the Euclidean manifold. Now, it is important to carefully translate the excised region from the continuum picture to the discrete one in order to reliably compare the volume profiles. For this we relate the physical parameters on both sides. In the continuum there are only two parameters, the mass M and the cosmological constant Λ, which sets the cosmological radius $R_0 = \sqrt{3/\Lambda}$. Newton's constant G_N has been set to one. In CDT simulations performed so far, the directly specifiable parameters[6] are Newton's constant, the mass, and the number of four-simplices N. The lattice spacing a is introduced to relate dimensionless simulation

[6] Another parameter specifiable in simulations is the directional asymmetry parameter Δ, though its value is not accessible in a classical geometry. For the discrete computations presented in this subsection, we will assume for definiteness that $\Delta = 0$, such that the Euclideanized four-simplices are all equilateral [32].

parameters to dimensionful physical parameters. We relate simulation and continuum parameters by comparing geometric observables in the continuum limit. For instance, for Euclidean de Sitter space, the total four-volume is $V_4 = \frac{8\pi^2}{3} R_0^4$, from (12), while on the triangulation side we have $V_4 = \frac{\sqrt{5}}{96} a^4 N$, leading to the relationship

$$a/R_0 = \left(\frac{8 \cdot 96\pi^2}{3\sqrt{5}} \right)^{1/4} N^{-1/4} \sim 5.8 N^{-1/4}. \tag{13}$$

Typical values of $N \sim 3 \times 10^5$ give $a/R_0 \sim 1/4$.

Another important relationship is between the lattice spacing a and the maximum mass M accessible to simulations. To find the possible range of masses we recall that the vacuum caustic boundary $R_* = 3M^{1/3} M_N^{2/3}$ must fall within the matter region, $R_* < R_S$. On the other hand, in order to compare directly with the calculations done in this paper, one should consider mass distributions that are sufficiently compact to fit inside a region of the same size as the simplex whose volume we neglect, that is $R_S < a$. The resulting condition $R_* \leq a$ can be expressed as an upper bound on the mass M:

$$M \;\leq\; 3^{3/2} \left(\frac{a}{R_0} \right)^3 M_N \;=\; \frac{1}{3} a^3 \Lambda \;\sim\; a \sqrt{\frac{8 \cdot 96\pi^2}{3\sqrt{5} N}} \;\sim\; 33.6 \frac{a}{\sqrt{N}}. \tag{14}$$

The first is the most useful form of the bound for the numerical calculations carried out in Appendix A and section 4.3, where, as we shall see, the dimensionless parameter $\epsilon = M/M_N$ determines the shape of the volume profiles, while the last gives an estimate for the maximum accessible mass in terms of simulation parameters, with the approximation coming from direct use of equation (13). Since a/R_0 is expected to be small, the deviations of the volume profile from the Euclidean de Sitter case for accessible masses are also likely to be small.

4.3 Derivation of the volume profiles

Having discussed the range of validity of the excision we can move on to the derivation of the volume profile which can be used to test the classical limit of matter-coupled CDT quantum gravity and constitutes the main result of our work. From the line element (7) and definition (4) we obtain an integral expression for the total three-volume of the vacuum region,

$$V_3(\tau) = 8\pi \int_{R_i^{\min}(\tau)}^{R_{++}} dR_i \frac{R^2(\tau, R_i) R'(\tau, R_i)}{\sqrt{f(R_i)}}, \tag{15}$$

where $R' = \partial R / \partial R_i$, a factor of 4π comes from the angular integration, and an extra factor of 2 takes the doubling of the $R_i \leq R_{++}$ region into account, as explained in section 3.3. The function $R_i^{\min}(\tau)$ is the cut-off condition $R = a$ in proper-time coordinates.

In the continuum, increasing the mass while keeping R_0 (and therefore the cosmological constant Λ) fixed changes the total four-volume. In CDT simulations, however, the four-volume (that is, the number of four-simplices) is usually kept fixed for technical reasons.[7] In order to facilitate comparison with CDT results, we invert the

[7] The path integrals for fixed four-volume and fixed cosmological constant are related by a Legendre transformation.

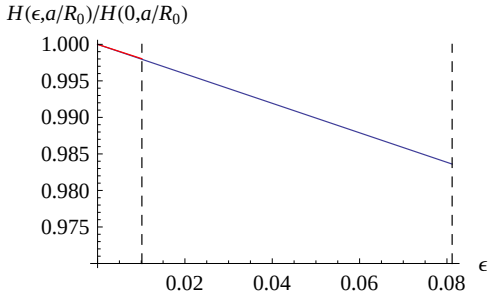

Figure 5: Plots of the dependence of the scaled total four-volume on the parameter ϵ for the two cut-off values $a/R_0 = 1/8$ [red line, ranging from zero to the first vertical line at $\epsilon = 3^{3/2}(1/8)^3$] and $a/R_0 = 1/4$ [blue line, ranging from zero to the second vertical line at $\epsilon = 3^{3/2}(1/4)^3$]. Both functions are normalized to one at $\epsilon = 0$. In the displayed region the curves are linear to very good approximation; the cut-off dependence is essentially negligible.

relationship between R_0 and V_4 in the continuum for fixed mass M. First, note that the function R in the definition of the volume profile (15) and the four parameters τ, R_i, M and R_0 on which it depends all have the dimension of length. Hence, we can write

$$R(\tau, R_i, M, R_0) = R_0 F(\zeta, R_i/R_0, \epsilon), \tag{16}$$

for some dimensionless function F that depends only on the dimensionless parameters $\zeta = \tau/R_0$, $\epsilon = M/M_N = 3^{3/2}M/R_0$ and the ratio R_i/R_0. The volume profile can therefore also be written as

$$V_3(\tau, \epsilon) = R_0^3 G(\tau/R_0, \epsilon), \tag{17}$$

with another dimensionless function G whose explicit form is to be evaluated. Note that the lower integration limit in (15) introduces an additional dependence on the lattice length a that we suppress here. From equation (12) it follows that $G(\zeta, 0) = 2\pi^2 \cos^3\zeta$ for the case $M = 0$. In terms of the function G the four-volume is

$$V_4(\epsilon) = \int_{-\tau_{\max}(\epsilon)}^{\tau_{\max}(\epsilon)} d\tau \; V_3(\tau, \epsilon) = R_0^4 \int_{-\tau_{\max}(\epsilon)/R_0}^{\tau_{\max}(\epsilon)/R_0} d\zeta \; G(\zeta, \epsilon) \equiv R_0^4 H(\epsilon). \tag{18}$$

In these expressions the integration limit is given by the time $\tau_{\max}(\epsilon)$ where the three-volume becomes zero. For Euclidean de Sitter space the value of the function $H(\epsilon)$ before cutting out the tube is $H(0) = 8\pi^2/3$. If V_4^* is the fixed four-volume used in a simulation, we have to adjust R_0 depending on the value of ϵ by setting $R_0(\epsilon) = (V_4^*/H(\epsilon))^{1/4}$. The rescaled four-volume $H(\epsilon)$ can be easily evaluated analytically in static coordinates:

$$\begin{aligned} H(\epsilon, a/R_0) = V_4/R_0^4 &= \frac{4\pi}{R_0^4} \int_0^{T_P} dT \int_a^{R_{++}} dR \; R^2 \\ &= \frac{8\pi^2}{3} \frac{8\cos^3(\alpha(\epsilon)/3) - 3^{3/2}(a/R_0)^3}{\left| \frac{3\epsilon}{4\cos^2(\alpha(\epsilon)/3)} - 6\cos(\alpha(\epsilon)/3) \right|}, \end{aligned} \tag{19}$$

where $f(R)$, R_{++}, T_P, and $\alpha(\epsilon) = \arccos(-\epsilon)$ were introduced in section 3.1. We checked the numerical evaluation of the volume profiles $V_3(\tau, \epsilon)$, as described below,

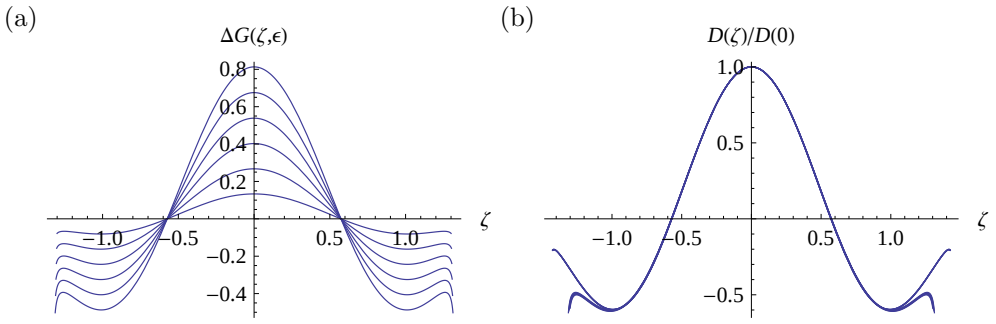

Figure 6: (a) Difference, $\Delta G(\zeta,\epsilon) = G(\zeta,0) - G(\zeta,\epsilon)$, between the pure EdS volume profile rescaled to a fixed four-volume and the rescaled volume profiles for $\epsilon = \epsilon_{\max}/7, \ldots, 6\epsilon_{\max}/7$, with cut-off at $R = a = R_0/4$ and $\epsilon_{\max} = 3^{3/2}(a/R_0)^3$. (b) Repeating the difference measurements of (a) for both $a/R_0 = 1/4$ and $a/R_0 = 1/8$ yields a total of 12 curves, which we have normalized by letting them all go through the point $(0,1)$. We observe that they are multiples of a single universal curve, modulo some weak cut-off artifacts near $\zeta = \pm\pi/2$ that quickly disappear for smaller values of a/R_0.

by comparing the value of $H(\epsilon, a/R_0)$ obtained from numerical quadrature of (18) to its exact value in (19) and found that our numerics are reliable.

For small a/R_0, and over the correspondingly small range of ϵ, the total four-volume is well approximated by

$$\frac{H(\epsilon, a/R_0)}{H(0, a/R_0)} \sim 1 - 3^{-3/2}\left[1 + 3(a/R_0)^3\right]\epsilon, \tag{20}$$

as can be seen from Fig. 5.

In Fig. 6a we have plotted the difference between the rescaled pure Euclidean de Sitter profile $G(\zeta,0)$ and the rescaled profiles $G(\zeta,\epsilon)$ for different values of $\epsilon > 0$, with the same interior region cut out, in the mass range given by (14) and for same fixed four-volume. They were obtained in Mathematica by first dividing the positive region of the τ-interval into 200 equidistant parts. For each τ the integral (15) is computed by numerical quadrature with the integrand given by cubic spline interpolation over 400 equidistant points. These points are obtained by solving numerically the implicit relation (30) for R and by finite differences to find R'. Having obtained the points of the $V_3(\tau,\epsilon)$ curve, we perform another cubic interpolation and numerically integrate the resulting function to get $H(\epsilon)$, according to (18). This allows us to rescale the profiles and obtain $G(\zeta,\epsilon)$ from equation (17). The curves in Fig. 6a appear to scale linearly in ϵ. Indeed, after a rescaling linear in ϵ, all of them collapse onto the single curve (modulo cut-off artifacts) plotted in Fig. 6b. Since we are restricted to small values of the parameter ϵ, it is not surprising that we are in the linear regime, where rescaled profiles are well approximated by the first two terms of the Taylor expansion in ϵ,

$$G(\zeta,\epsilon) = 2\pi^2\cos^3\zeta - \epsilon D(\zeta) + O(\epsilon^2). \tag{21}$$

In Fig. 6b we show $D(\zeta)/D(0)$, that is, the linear coefficient in (21), normalized such that its value at $\zeta = 0$ is given by 1.

Numerical simulations produce volume profiles $V_3(\tau)$ in lattice units. Rescaling the range of τ to $[-\pi/2, \pi/2]$ fixes the value of R_0 in lattice units and defines the rescaled volume profile $G(\zeta)$ through equation (17). We believe that subtracting $G(\zeta)$ from $2\pi^2\cos^3\zeta$ and normalizing this difference to be 1 at $\zeta = 0$ should reproduce

the curve $D(\zeta)/D(0)$ plotted in Fig. 6b, thereby establishing a good classical limit of matter-coupled CDT. The corresponding value of ϵ can be obtained from comparing the normalized simulation four-volume V_4^*/R_0^4 to $H(\epsilon)$ in (19) or (20).

5 Conclusions and Outlook

In any theory of quantum gravity, it is notoriously difficult to come up with "observables", that is, quantities with an invariant geometric meaning, which may eventually be related to physical observations. Besides their obvious use in bridging between theory and phenomenology, they play an important role at the current stage, when we are not yet in possession of a complete, nonperturbative formulation of quantum gravity. This role is at least two-fold. First, appropriately coarse-grained geometric observables can provide nontrivial tests of whether a proposed nonperturbative theory possesses a well-defined classical limit, and whether in this limit it reproduces the physics of classical general relativity correctly. Second, evaluating an observable which explicitly probes the quantum regime of the theory can be a means of comparing different candidate theories of quantum gravity.

A prominent example of both of these uses is the so-called spectral dimension of spacetime, measured on short and large scales. Its expectation value was first studied in Causal Dynamical Triangulations [2, 10], exhibiting a characteristic scale dependence. On large scales, the expected classical value of four is reproduced, which decreases to two[8] when approaching the Planck scale, indicating strong deviations from classicality. This is a highly nontrivial result which has since been reproduced in at least two completely different formulations of quantum gravity [46, 47], stimulating further research into a common origin of this seemingly universal behaviour [48, 49].

This example illustrates how observables of this type can yield valuable information about the quantum theory. Unfortunately, they are rather rare. In the present work, we have looked at another geometric quantity which has been studied previously in CDT, the three-volume profile, which makes explicit use of the proper-time foliation. In a first attempt to try and quantify the effects of matter on geometry in this framework, we have analyzed how the volume profile can be expected to change under insertion of a point-like mass, as a function of the particle mass M, if the corresponding ground state geometry which is generated dynamically by CDT is related to the Schwarzschild-de Sitter geometry.

As we have seen, the analysis involved several nontrivial steps, despite the relatively simple and static nature of the classical metric. The difficulties have to do with the nonlocal nature of the volume profile, which requires a careful treatment of boundary conditions and regions of validity of the coordinate systems one has to use in a continuum calculation. Another difficulty derives from having to define a quantity which is geometric, i.e., independent of any particular coordinate choice, to be able to compare with the (coordinate-free) set-up of the CDT simulations. Both of these issues are characteristic for quantum observables in gravity.

Our specific construction involved the use of a system of Gaussian normal coordinates. On the one hand, this gave us a relatively good control on some of the global properties of the Euclidean Schwarzschild-de Sitter space like at the (Euclideanized) cosmological horizon, on the other hand the coordinates do not cover the complete

[8] More precisely, a value compatible with two, taking into account the error bars of the Monte Carlo simulations.

region outside the source. However, when restricting the mass to be small, the proper-time foliation is nearly global in the sense that neglecting the contribution to the spatial volume from the region inside of a certain small Schwarzschild radius, we obtain an approximation to the actual volume profiles while preserving their characteristic deviation from the Euclidean de Sitter profile. The approximation is equivalent to neglecting those simplices that contain the mass-line when determining the average spatial volume in the computer simulations. Let us point out that the deviations we have computed are small and one will need good control of the numerical errors to measure them. We also found that the correct way of implementing the mass line in the simulations, if one wants to compare to our calculation, is by representing it by a closed contractible loop on the geometry which has a four-sphere topology.

We regard the present work as a step towards understanding the dynamics of coupled systems of matter and geometry in nonperturbative quantum gravity, about which there is currently little known, since most candidate theories have focussed their efforts on the pure-gravity situation. As we have already mentioned above, it is possible that our treatment can be improved, to cover a larger region of spacetime and/or the case of larger masses. In addition, it would be interesting to derive the volume fluctuations from a mini-superspace action in the same way as has been done for Euclidean de Sitter space [4] and check whether the agreement between the analytical and numerical calculations persists.

Acknowledgements. We thank T. Budd, S. Butt and A. Görlich for discussion.— R.L. and P.R. were partially supported through the European Network on Random Geometry ENRAGE, contract MRTN-CT-2004-005616. R.L. acknowledges support by the Netherlands Organisation for Scientific Research (NWO) under their VICI program. I.K. was supported by the National Science and Engineering Research Council of Canada (NSERC).

A Geodesics in ESdS space

In this appendix we derive the line element on Euclidean Schwarzschild-de Sitter space in terms of Gaussian normal coordinates, Eq. (7), starting from the static form, Eq. (5). For this we first determine the radial geodesic equations for ESdS space.[9] The Killing vector $\xi = \partial/\partial T$ yields a conserved quantity along the geodesics,

$$E = g_{\mu\nu}\xi^\mu \frac{dx^\nu}{d\tau} = f(R)\dot{T}, \tag{22}$$

where the dot refers to differentiation with respect to τ. We will refer to E as the energy parameter. The geodesic equations are then

$$\frac{dR}{d\tau} = m\sqrt{f(R) - E^2}, \qquad \frac{dT}{d\tau} = \frac{E}{f(R)}, \tag{23}$$

where the $m = \pm 1$ distinguishes motion in Euclidean proper-time τ with increasing and decreasing R. Combining the two geodesic equations we find the proper time

[9] The complete analytic solution for geodesics in Schwarzschild-de Sitter space was constructed in [50, 51].

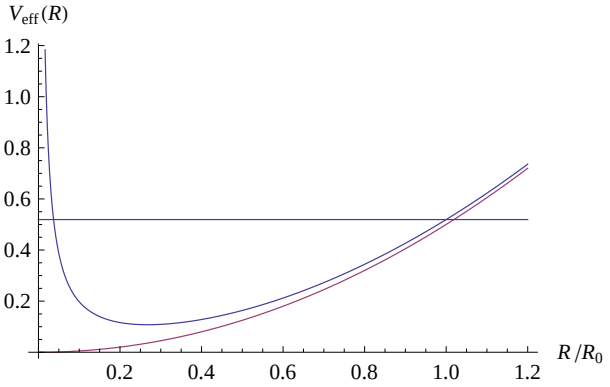

Figure 7: The effective potential for radial geodesic motion in ESdS space for $M = M_N/10$ (upper curve with horizontal line to illustrate turning points for the maximum total energy) and for $M = 0$ (lower curve). These potentials determine the evolution of the $R_i = const$ geodesics which form the proper-time coordinate system.

element along each geodesic,

$$d\tau = EdT + m\frac{\sqrt{f(R) - E^2}}{f(R)}dR. \tag{24}$$

While E is constant on a given geodesic, it may assume different values on different geodesics. For now, we take it as a yet to be specified function of coordinates $E(T, R)$. If we consider the two-dimensional R-T-plane to be foliated by non-intersecting geodesics, we can eliminate the T-coordinate in favour of their proper time τ and obtain the metric [52]

$$ds^2 = d\tau^2 + \frac{1}{E(T(\tau, R), R)^2}\left(dR - m\sqrt{f(R) - E(T(\tau, R), R)^2}d\tau\right)^2 + R^2 d\Omega^2. \tag{25}$$

Note that the metric is already in proper-time form. To set the shift vector to zero, and obtain a Gaussian normal coordinate system, we replace the R-coordinate by a comoving radial coordinate. We introduce the comoving radial coordinate by first observing that radial geodesic motion of a test body in ESdS space corresponds to motion in the effective potential

$$V_{\rm eff}(R) = M/R + R^2/2R_0^2 \tag{26}$$

with total energy $E_{\rm tot} = (1 - E^2)/2$. This is easily seen from writing the equation in the form $\frac{1}{2}\dot{R}^2 + V_{\rm eff}(R) = E_{\rm tot}$. The potential is displayed in Fig. 7 for $M = 0$ and $M = M_N/10$. It has a minimum at $R = R_* = M^{1/3}R_0^{2/3}$. A test body has two turning points given by the roots of the equation $f(R) = E^2$. The larger turning radius, R_i, will be our comoving radial coordinate. For the maximal energy $E_{\rm tot} = 1/2$ the turning radii are the two horizons, $R = R_+$ and $R = R_{++}$. Hence, for the construction of coordinates in proper-time gauge we look at geodesic motion of test bodies with initial positions $R_* < R_i < R_{++}$ and zero initial velocity. The synchronization condition that each geodesic passes through its turning point at $T = \tau = 0$ completes the specification of the proper-time coordinates (τ, R_i). In terms of the new coordinates, the energy parameter is specified simply as $E = \sqrt{f(R_i)}$.

Integration of the radial geodesic equation yields

$$\tau(R, R_i) = -m \int_R^{R_i} \frac{dy}{\sqrt{f(y) - f(R_i)}} = -mR_0 \int_\rho^1 d\xi \sqrt{\frac{\xi}{P(\xi)}}, \tag{27}$$

with the dimensionless quantities $\xi = y/R_i$, $\rho = R/R_i \leq 1$, $\beta = 54MM_N^2/R_i^3$ and

$$P(\xi) = -\xi^3 + (\beta + 1)\xi - \beta = (1 - \xi)(\xi - \xi_+)(\xi - \xi_-), \tag{28}$$

$$\xi_\pm = -\frac{1}{2} \pm \Delta, \quad \Delta = \sqrt{\frac{1}{4} + \beta}. \tag{29}$$

In terms of special functions the above integral becomes

$$\tau = -mR_0 \sqrt{2/\Delta} \left[(1 - \xi_-)\Pi(\mu, \frac{\xi_+ - 1}{2\Delta}, r) + \xi_- F(\mu, r) \right], \tag{30}$$

where

$$\mu = \arcsin \sqrt{\frac{2\Delta(1 - \rho)}{(1 - \xi_+)(\rho - \xi_-)}}, \quad r = \sqrt{\frac{(1 - \xi_+)(-\xi_-)}{2\Delta}}. \tag{31}$$

F and Π are the elliptic functions of the first and third kind, respectively [53, 3.167.15]. Equation (30) is an implicit definition of $R(\tau, R_i)$. This relation allows us to write the line element in terms of proper-time τ and comoving spatial coordinate R_i as

$$ds^2 = d\tau^2 + \frac{(\partial R/\partial R_i)^2}{f(R_i)} dR_i^2 + R(\tau, R_i)^2 d\Omega^2. \tag{32}$$

When $M = 0$, the expression for $R(\tau, R_i) = R_i \cos(\tau/R_0)$ is known explicitly. When $M \neq 0$, the values of $R(\tau, R_i)$ can be obtained by numerically solving the implicit equation (30). Both cases are shown for comparison in Fig. 8. Note that the radial geodesics in EdS space, Fig. 8a, do not intersect except for extreme values of τ, but those in ESdS space do, Fig. 8b, that is, they form caustics. The implications of these caustics are discussed in section 3.3.

B Caustic formation in an interior matter solution

We show here that gluing the vacuum ESdS solution to an interior solution of matter of constant density does not significantly improve on the situation found in vacuo with respect to the formation of caustics in a set of Gaussian normal coordinates. The matter distribution we are interested in is the Wick-rotated version of a simple model of a spherically symmetric relativistic star in the presence of a positive cosmological constant. The Euclidean stress-energy tensor can be taken to be the one of a perfect fluid with a uniform density ρ,

$$T^{\mu\nu} = -\left(p(R) + \rho\right) u^\mu u^\nu + p(R) g^{\mu\nu}. \tag{33}$$

Solving the Euclidean Einstein equations one finds that the line element inside the star written in Schwarzschild coordinates is [54][10]

$$ds^2 = \left(A\, Y(R_S) - B\, Y(R)\right)^2 dT^2 + \frac{dR^2}{Y(R)^2} + R^2 d\Omega^2, \tag{34}$$

[10]Some intermediate results in this reference contain typographical errors. However, we have verified that the formulas relevant for this work are correct.

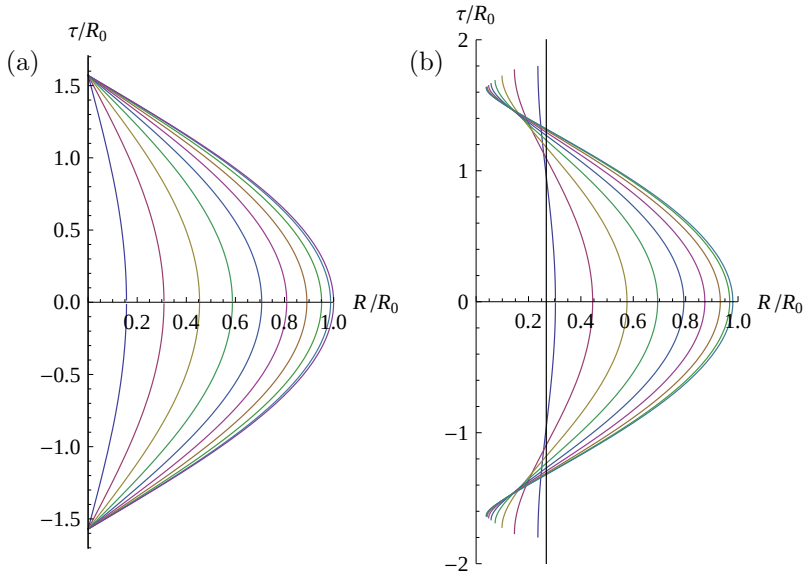

Figure 8: $R_i = const$ geodesics in (a) Euclidean de Sitter space and (b) Euclidean Schwarzschild-de Sitter ($M = M_N/10$) space. The outermost line is the $R_i = R_{++}$ geodesic. (a) All curves converge at $\tau = \pm\pi R_0/2$. (b) The vertical line marks $R = R_* \equiv M^{1/3}R_0^{2/3}$, the minimum of the effective potential. Geodesics, which at $T = 0$ are located to the right of the line start intersecting each other when entering the region $R < R_*$, forming caustics. There are no caustics in the region $R_* < R < R_{++}$.

where we denote the location of the surface of the star by $R_S > R_+$ (or $R_S > R_*$, as we restrict to later on) and define

$$Y(R) = \sqrt{1 - \frac{8\pi\rho + \Lambda}{3}R^2}, \quad A = \frac{9M}{6M + \Lambda R_S^3}, \quad B = \frac{3M - \Lambda R_S^3}{6M + \Lambda R_S^3}, \quad \rho = \frac{3M}{4\pi R_S^3}. \tag{35}$$

Setting $R = R_S$ in (34), we see that the interior matter solution is matched continuously to the exterior ESdS vacuum region. This implies that the correct matching condition for the radial timelike geodesics is that the first derivatives match at the surface of the star.

For the case $R_S = R_* = M^{1/3}R_0^{2/3}$ we can determine the extension of radial geodesics to the interior region explicitly. This is depicted in Fig. 9a. The geodesics intersect inside of the matter region and hence the formation of caustics persists.

This result is not specific to the choice $R_S = R_*$. In order to avoid a lengthy analysis we set up a simple criterion for the intersection of geodesics. We release two test bodies, one from $R_i = R_{++}$ and the other from $R_i = R_S$, with zero initial velocity and compare the proper time they take to arrive at $R = 0$, which is the centre of the star. If the test body starting at the surface takes longer, then there must be an intersection. The arrival time for the test body starting from $R_i = R_{++}$ is given by

$$\tau(R_i = R_{++}) = \sigma \arcsin\left(R_S/\sigma\right) + \int_{R_S}^{R_{++}} \frac{dy}{\sqrt{f(y)}}, \tag{36}$$

with $1/\sigma^2 = \left(1 + 2/\gamma^3\right)/(27M_N^2)$ and $\gamma = R_S/R_*$. The first term in (36) constitutes

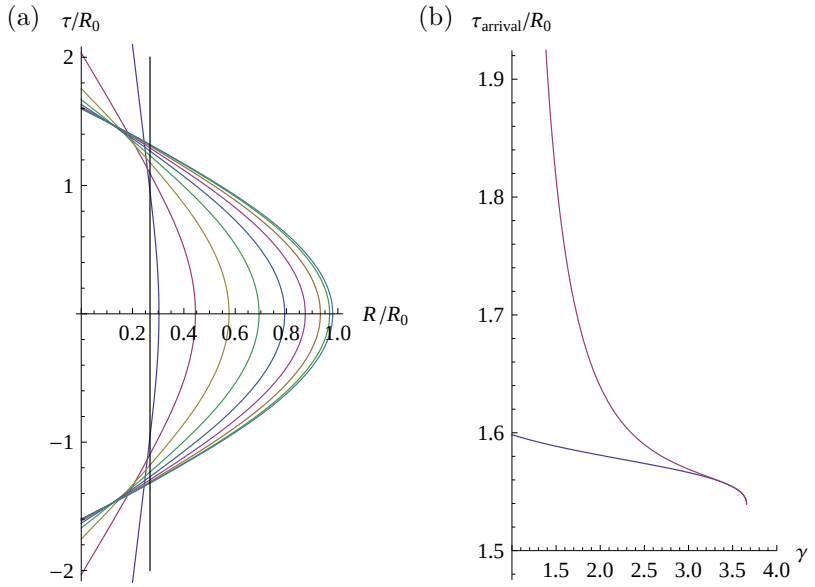

Figure 9: Gluing an interior uniform matter distribution to an external Euclidean Schwarzschild-de Sitter solution for $M = M_N/10$. (a) $R_i = const$ geodesics for the special case of gluing at the radius $R = R_*$ (vertical line). The curves intersect inside the matter region, illustrating the breakdown of the Gaussian normal coordinates. The outermost line is the $R_i = R_{++}$ geodesic. (b) For general gluing radius: proper time at $R = 0$ (arrival time) of the two radial geodesics, $R = R_{++}$ (lower curve) and $R = \gamma R_*$ (upper curve), as functions of $\gamma = R_S/R_*$, showing that adjusting the gluing condition does not prevent the breakdown of the Gaussian coordinates in the interior region.

the contribution of the matter region and the second constitutes that of the vacuum region. The integral in the second term is the same as that evaluated in (30).

For the test body starting with zero initial velocity at the star's surface, $R = R_S$, we have

$$\tau(R_i = R_S) = \int_0^{R_S} \frac{dy}{Y(y)\sqrt{1 - \frac{f(R_S)}{(AY(R_S) - BY(y))^2}}}, \tag{37}$$

where the constants $A, B, f(R_S)$ and $Y(R_S)$ all depend on γ. The resulting arrival times are plotted in Fig. 9b, where the upper curve represents the $R_i = R_S$ case and was found by numerical integration. The arrival times are equal only when the trajectories coincide, i.e., when the star surface reaches the cosmological horizon. Therefore, we conclude that the Gaussian normal coordinates are not well defined in the interior region for any choice of radius and density of the mass distribution. We have not investigated whether fine-tuning of the internal structure of the matter model (e.g. by considering inhomogeneous or anisotropic fluids) could help in preventing the occurrence of caustics. However, such a possibility appears unlikely to us.

References

[1] J. Ambjørn, J. Jurkiewicz and R. Loll. Emergence of a 4D world from causal quantum gravity. *Phys. Rev. Lett.*, 93:131301, 2004.

[2] J. Ambjørn, J. Jurkiewicz and R. Loll. Spectral dimension of the universe. *Phys. Rev. Lett.*, 95:171301, 2005.

[3] J. Ambjørn, A. Görlich, J. Jurkiewicz and R. Loll. Planckian birth of the quantum de Sitter universe. *Phys. Rev. Lett.*, 100:091304, 2008.

[4] J. Ambjørn, A. Görlich, J. Jurkiewicz and R. Loll. The nonperturbative quantum de Sitter Universe. *Phys. Rev.*, D78:063544, 2008.

[5] J. Ambjørn, Z. Burda, J. Jurkiewicz and C.F. Kristjansen. 4-d quantum gravity coupled to matter. *Phys. Rev.*, D48:3695–3703, 1993.

[6] S. Bilke, Z. Burda, A. Krzywicki, B. Petersson, J. Tabaczek and G. Thorleifsson. 4d simplicial quantum gravity interacting with gauge matter fields. *Phys. Lett.*, B418:266–272, 1998.

[7] J. Ambjørn, J. Jurkiewicz, S. Bilke, Z. Burda and B. Petersson. Z(2) gauge matter coupled to 4-D simplicial quantum gravity. *Mod. Phys. Lett.*, A9:2527–2542, 1994.

[8] J. Ambjørn, K.N. Anagnostopoulos and J. Jurkiewicz. Abelian gauge fields coupled to simplicial quantum gravity. *JHEP*, 08:016, 1999.

[9] S. Horata, H.S. Egawa, N. Tsuda and T. Yukawa. Phase structure of four-dimensional simplicial quantum gravity with a u(1) gauge field. *Progress of Theoretical Physics*, 106(5):1037–1050, 2001.

[10] J. Ambjørn, J. Jurkiewicz and R. Loll. Reconstructing the universe. *Phys. Rev.*, D72:064014, 2005.

[11] S. Carlip. *Quantum Gravity in 2+1 Dimensions*. Cambridge University Press, December 2003.

[12] A. Staruszkiewicz. Gravitation theory in three-dimensional space. *Acta Phys. Polon.*, 24:735–740, 1963.

[13] S. Deser, R. Jackiw and G. 't Hooft. Three-dimensional Einstein gravity: Dynamics of flat space. *Ann. Phys.*, 152:220, 1984.

[14] G. 't Hooft. Quantization of point particles in 2+1 dimensional gravity and space-time discreteness. *Class. Quant. Grav.*, 13:1023–1040, 1996.

[15] H.-J. Matschull and M. Welling. Quantum mechanics of a point particle in 2+1 dimensional gravity. *Class. Quant. Grav.*, 15:2981–3030, 1998.

[16] K. Noui and A. Perez. Three dimensional loop quantum gravity: Coupling to point particles. *Class. Quant. Grav.*, 22:4489–4514, 2005.

[17] L. Freidel and D. Louapre. Ponzano-Regge model revisited. I: Gauge fixing, observables and interacting spinning particles. *Class. Quant. Grav.*, 21:5685–5726, 2004.

[18] V. Husain and O. Winkler. Quantum resolution of black hole singularities. *Class. Quant. Grav.*, 22:L127–L134, 2005.

[19] V. Husain and O. Winkler. Quantum black holes from null expansion operators. *Class. Quant. Grav.*, 22:L135–L142, 2005.

[20] V. Husain and O. Winkler. Flat slice Hamiltonian formalism for dynamical black holes. *Phys. Rev.*, D71:104001, 2005.

[21] A. Gomberoff and C. Teitelboim. de Sitter black holes with either of the two horizons as a boundary. *Phys. Rev.*, D67:104024, 2003.

[22] P.H. Ginsparg and M.J. Perry. Semiclassical perdurance of de Sitter Space. *Nucl. Phys.*, B222:245, 1983.

[23] R. Bousso. Proliferation of de Sitter space. *Phys. Rev.*, D58:083511, 1998.

[24] M. Spradlin, A. Strominger and A. Volovich. Les Houches lectures on de Sitter space. In Bachas, C.P.; Bilal, A.; Douglas, M.R.; Nekrasov, N.A.; David, F., editor, *Unity from Duality: Gravity, Gauge Theory and Strings*, volume 76 of *Les Houches Summer School*, pages 423–454. Springer, 2003.

[25] J. Ambjørn, A. Görlich, J. Jurkiewicz and R. Loll. The universe from scratch. *Contemp. Phys.*, 47:103–117, 2006.

[26] J. Ambjørn, A. Görlich, J. Jurkiewicz and R. Loll. Quantum gravity, or the art of building spacetime. In D. Oriti, editor, *Approaches to Quantum Gravity: Toward a New Understanding of Space, Time and Matter*, pages 341–359. Cambridge University Press, 2009.

[27] J. Ambjørn, A. Görlich, J. Jurkiewicz and R. Loll. Quantum gravity as sum over spacetimes. In Booß-Bavnbek, B.; Esposito, G.; Lesch, M., editor, *New Paths Towards Quantum Gravity*, volume 807 of *Lecture Notes in Physics*, pages 59–124. Springer, 2010.

[28] J. Ambjørn, A. Görlich, J. Jurkiewicz and R. Loll. Causal dynamical triangulations and the quest for quantum gravity. In Ellis, G.; Murugan, J.; Weltman, A., editor, *Foundations of Space and Time*. Cambridge University Press, 2010. (to appear).

[29] R. Loll. The emergence of spacetime, or, quantum gravity on your desktop. *Class. Quant. Grav.*, 25:114006, 2008.

[30] G.W. Gibbons (ed.) and S.W. Hawking (ed.). *Euclidean Quantum Gravity*. World Scientific, Singapore, Singapore, 1993.

[31] J. Ambjørn, J. Jurkiewicz and R. Loll. Nonperturbative Lorentzian path integral for gravity. *Phys. Rev. Lett.*, 85:924–927, 2000.

[32] J. Ambjørn, J. Jurkiewicz and R. Loll. Dynamically triangulating Lorentzian quantum gravity. *Nucl. Phys.*, B610:347–382, 2001.

[33] J. Ambjørn and J. Jurkiewicz. Four-dimensional simplicial quantum gravity. *Phys. Lett.*, B278:42–50, 1992.

[34] T. Regge. General relativity without coordinates. *Nuovo Cim.*, 19:558–571, 1961.

[35] J. Ambjørn and R. Loll. Non-perturbative Lorentzian quantum gravity, causality and topology change. *Nucl. Phys.*, B536:407–434, 1998.

[36] B. Dittrich and R. Loll. Counting a black hole in Lorentzian product triangulations. *Class. Quant. Grav.*, 23:3849–3878, 2006.

[37] K.S. Thorne, C.W. Misner and J.A. Wheeler. *Gravitation.* Physics Series. W. H. Freeman, 2nd printing edition, September 1973.

[38] C. Teitelboim. Quantum mechanics of the gravitational field. *Phys. Rev.*, D25:3159, 1982.

[39] C. Teitelboim. The proper time gauge in quantum theory of gravitation. *Phys. Rev.*, D28:297, 1983.

[40] R.M. Wald. *General Relativity.* University of Chicago Press, first edition, June 1984.

[41] R. Steinbauer and J.A. Vickers. The use of generalised functions and distributions in general relativity. *Class. Quant. Grav.*, 23:R91–R114, 2006.

[42] H. Nariai. On a new cosmological solution of Einstein's field equations of gravitation. *Sci. Rep. Tohoku Univ.*, 35:46, 1951. reprinted in *Gen. Rel. Grav.* 31:963, 1999.

[43] F.-L. Lin and C. Soo. Quantum field theory with and without conical singularities: black holes with a cosmological constant and the multi-horizon scenario. *Class. Quant. Grav.*, 16(2):551–562, 1999.

[44] R. Gautreau. Geodesic coordinates in the de Sitter universe. *Phys. Rev. D*, 27:764, 1983.

[45] R. Gautreau. On Kruskal-Novikov co-ordinate systems. *Nuovo Cim.*, 56B:49, 1980.

[46] O. Lauscher and M. Reuter. Fractal spacetime structure in asymptotically safe gravity. *JHEP*, 10:050, 2005.

[47] P. Hořava. Spectral dimension of the universe in quantum gravity at a Lifshitz point. *Phys. Rev. Lett.*, 102:161301, 2009.

[48] S. Carlip. Spontaneous dimensional reduction in short-distance quantum gravity? In Kowalski-Glikman, J.; Durka, R.; Szczachor, M., editor, *The Planck Scale: Proceedings of the XXV Max Born Symposium*, volume 1196, pages 72–80. AIP, 2009.

[49] J. Ambjørn, A. Görlich, S. Jordan, J. Jurkiewicz and R. Loll. CDT meets Horava-Lifshitz gravity. *Phys. Lett.*, B690:413–419, 2010.

[50] E. Hackmann and C. Lämmerzahl. Complete analytic solution of the geodesic equation in Schwarzschild- (Anti-) de Sitter spacetimes. *Phys. Rev. Lett.*, 100:171101, 2008.

[51] E. Hackmann and C. Lämmerzahl. Geodesic equation in Schwarzschild- (anti-) de Sitter space-times: Analytical solutions and applications. *Phys. Rev.*, D78:024035, 2008.

[52] K. Martel and E. Poisson. Regular coordinate systems for Schwarzschild and other spherical spacetimes. *Am. J. Phys.*, 69:476–480, 2001.

[53] I.S. Gradshteyn and I.M. Ryzhik. *Table of Integrals, Series and Products*. Elsevier Inc., 7th edition, 2007.

[54] Z. Stuchlik. Spherically symmetric static configurations of uniform density in spacetimes with a non-zero cosmological constant. *Acta Phys. Slov.*, 50:219–228, 2000.